# Experimental and modelling studies on HVO-methanol mixtures separation for superyachts applications

La Colla, E.; van Biert, L.; Grenko, B.; Loeff, Giedo

# Experimental and modelling studies on HVO-methanol mixtures separation for superyachts applications

Ir. E La Colla[a*], Dr. Ir. L. van Biert[a], B. Grenko, MSc[a], Ing. G Loeff[b]

[a]*Delft University of Technology, Mekelweg 5, Delft, 2628 CD, The Netherlands;* [b]*Feadship - De Voogt Naval Architects, Hoofddorp, 2132 JK, The Netherlands*

*Corresponding author. Email: ernestolacolla@hotmail.it

### Synopsis

A growing concern is associated to the greenhouse gases emissions of superyachts, consequently alternative fuels are introduced to the market. For the yachting decarbonisation, this work focuses on hydrotreated vegetable oil (HVO) and methanol. Nevertheless, the uncertain global availability of these fuels can undermine the operations of ocean-crossing superyachts. Thus, a multi-fuel system is installed allowing for fuels switchover and built-in flexibility. Moreover, non-dedicated tanks are installed for the alternative storage of HVO and methanol to make optimal use of the tanks' capacity. However, the alternative storage of HVO and methanol causes mutual fuels' contamination. The lack of standards and research on accepted fuels impurity makes full fuels' separation relevant to be explored. In this work, to avoid degradation of dual-fuel engines or fuel cells, gravity-settling tanks and disc-bowl centrifuges were studied to separate HVO-methanol mixtures. Shake tests were conducted on HVO-methanol mixtures to quantify the separation time and relative concentrations to obtain complete gravity separation. The gravity tests revealed methanol traces in HVO for all the tested mixtures within the 1 hour-3 days observation time, due to the low-density difference between the fuels. This makes the use of gravity-settling tanks impractical onboard for quasi-instantaneous fuels supply to the converters. A mathematical model was developed for disc-bowl centrifuges to assess the separator performance and separation time. Furthermore, the centrifuge was sized by providing the separator working conditions for varying engine modes. Moreover, spin tests were conducted to validate the mathematical model. The model showed that full separation is achievable with a larger centrifuge compared to existing designs. The larger design is due to the low-density difference between the fuels. The maximum separation time ranges from 5-10 minutes. Nevertheless, all the tested mixtures with the spin tests failed at achieving a state of full separation due to the dilution of a certain residual volume in the continuous liquid. The discrepancy between the mathematical model and the spin test results can lie in the neglected diluted phase of the dispersed fuel in the continuous liquid in the mathematical model. However, the mathematical model is a good tool to simulate the dynamic behaviour of the dispersed droplets. Consequently, the onboard use of a centrifuge for separating HVO-methanol mixtures should be evaluated by quantifying the concentration of the fuels' mixture entering the separator tailored per yacht. Furthermore, tests on dual-fuel engines or fuel cells are recommended to establish tolerable limits of fuel's contamination.

*Keywords:* Centrifuge, HVO, Liquid-liquid separation, Methanol, Superyachts

## 1 Introduction

Ships emit approximately 1076 million tonnes of $CO_2$, representing 3% of the global greenhouse gas (GHG) emissions (European Commission, n.a.), while superyachts emit yearly about 5 Mt of $CO_2$ equivalent (Kries, 2021). The International Maritime Organisation (IMO) aims to reduce ship-released $CO_2$ by 40% by 2030 compared to 2008 and achieve zero GHG emissions by 2050 (IMO, 2023). The IMO identified alternative fuels as a prevention for harmful emissions release (IMO, 2022). To cut yachts' emissions, *Feadship* largely researched hydrogen (Siepmann, 2019; Lambregts, 2021), hydrotreated vegetable oil (HVO) (van der Vliet, 2021), methanol (Kries, 2021) and hybrid propulsion (Visser, 2021). Despite the positive features of these alternative fuels, their large-scale availability is uncertain in the near term.

To overcome this challenge, a multi-fuel system enables refuelling alternative fuels where possible today, with diesel representing a viable option while alternative fuels become increasingly available. HVO and methanol were prioritised among alternative fuels for the relatively high readiness level of associated energy converters, market uptake and reduced emissions.

In a multi-fuel system, HVO and methanol can be alternatively stored in all tanks to make optimal use of the tanks' capacity. Additionally, dual-fuel (DF) engines and proton exchange membrane (PEM) fuel cells are

selected. Nevertheless, when storing multiple fuels in the same tank alternatively, fuels' contamination occurs. In DF engines contamination can yield wear and corrosion (Washecheck, P. H., Liu, A. T. C., Kennedy, E. F., 1983; Estefan and Brown, 1990; Cheung et al., 2009; Hazar and Temizer, 2012; Nautiyal et al., 1989), while fuel cells can be permanently damaged (Sterchi, 2001). However, research lacks specific mixture studies and marine quality standards. Hence, limits of HVO-methanol mutual contamination remains undefined for their usage in DF engines and fuel cells, making full HVO-methanol separation relevant to be explored.

The separation systems' selection depends on the mixture formed in storage tanks. Gravity-settling tanks or centrifuges can be used given the properties of HVO/methanol (Green and Perry, 2008) and their usage in existing vessels (McGeorge, 1998; Taylor, 1996). Specifically, disk-bowl types are chosen among centrifuges. Nevertheless, uncertainties remain on the separation efficacy and the required separation time.

Concerning gravity, generally, a 0.1-difference in specific gravity in a binary mixture sufficiently ensures phase separation (Kerr, 2007). Conversely, HVO and methanol have a maximum specific gravity difference of 0.03 (Ellis and Tanneberger, 2015; Neste, 2020). Moreover, the phase separation time of HVO-methanol mixtures is unclear (Kato et al., 1991). This might generate concerns for required high processing flows onboard. Consequently, if low settling rates are anticipated, centrifuges are identified as an alternative technique (Sorsamäki and Nappa, 2015; Green and Perry, 2008; B. Vermeire, 2021).

Effectiveness of disc-stack centrifuges is challenged by fuel density. Methanol and HVO densities differ by up to 30.5 kg/m$^3$ and possibly overlap (Ellis and Tanneberger, 2015; Neste, 2020). Literature is inconsistent on the minimum density difference allowing complete separation (Flottweg SE, n.a.; ECHA, n.a.; Towler and Sinnott, 2013; Green and Perry, 2008), leaving uncertainties on methanol-HVO separation effectiveness. This is enforced by lack of tests on these fuels and influence of tailored separator design parameters on performance (Dolphin Centrifuge, 2020). Thus, the separator sizing and its performance assessment are fundamental for separating HVO-methanol mixtures.

Literature shows lack of research on HVO-methanol mixtures separation, inconsistency between parameters to predict full separation and undefined separation time. This study investigates the efficacy of gravity-settling tanks and centrifuges as separation systems, alongside the time required for full separation. For gravity-settling tanks, phase separation tests are conducted. Regarding centrifuges, a centrifugal model is computed and spin tests performed for validation.

## 2 Methodology

This section presents methodologies for gravity-separation and centrifugation to determine HVO-methanol separation effectiveness.

### 2.1 Gravity separation

For gravity-settling tanks, experiments are performed on HVO-methanol mixtures to determine the time required by the fuels to fully separate by gravity.

Tests were performed on HVO and methanol with specifications as per Table 1. A camera placed in front of the beakers recorded the volume variation relative to a millilitres-scaled beaker. The camera helped detecting a transition from cloudy to clear appearance, indicating a shift from a single-homogeneous to binary phase. A light microscope was used to identify methanol droplets in HVO and measure their diameter, impacting dispersed liquid coalescence (Frising et al., 2008; Kamp et al., 2016) and exhibiting an inverse relationship with the settling time (De Haan et al., 2020; Ishii and Zuber, 1979; Richardson and Zaki, 1954).

The procedure followed is:

- The fuels were poured into a beaker at different concentrations relative to a fixed mixture's total volume. The mixture's total volume equals 100 ml and the tests were conducted on methanol at 1, 5, 10-70% v/v and 20°C.

- Fuels were mixed with a magnetic stirrer. The rotational speed of the magnetic stirrer was set at 1200 rpm and the stirring time at 1 minute, based on (Green and Perry, 2008).

- Liquid samples were removed from the beaker. To monitor the mixture's behaviour over time, samples were extracted after 5, 30 and 60 minutes. Extraction was conducted with a Pasteur pipette from half the height of the light phase for results' consistency.

- The samples were transferred to slide chambers to be observed at the microscope.

### 2.2 Centrifugal separation

Disc-bowl centrifuges are mathematically modelled as an alternative technology to gravity-settling tanks. Spin tests are conducted to validate this model.

Table 1: Main specifications of used HVO and methanol for phase-separation tests
(* at 15°C, ** at 20°C)

| Parameter | Unit | HVO | Methanol |
|---|---|---|---|
| Colour (appearance) | [-] | Colourless (Clear and bright) | Colourless (pale) |
| Relative density | [-] | 0.7811* | 0.7927** |
| Purity on dry basis | [% m/m] | - | 99.97 |
| Water | [% m/m] | 0.04 | 0.005 |
| Sulfur | [mg/kg] | < 3 | 4 |
| FAME | [% v/v] | < 0.05 | - |
| Total aromatic hydrocarbons | [% m/m] | < 0.2 | - |
| Kinematic viscosity | [m$^2$/s] | $3.127 \cdot 10^{-6}$ | - |
| Dynamic viscosity | [Ns/m$^2$] | - | $0.54 \cdot 10^{-3}$ |

### 2.2.1 Mathematical model

The mathematical model of the disc-stack centrifuge outputs the time required by the separator to start its operations and the separator performance. The time refers to the starting time for a continuously operating centrifuge. The separator performance assessment aims at full separation. Furthermore, the centrifuge outlet flows are inputs for this problem, influencing the fuels flow exiting the separator. Their values are constrained to match the fuel flows required by the engines onboard.

The model is computed using two methods: one observes the trajectory of heavy-fuel droplets, while the other focuses on the interface position variation within the disc-bowl formed by the two liquids.

Regarding the droplets' trajectory, the motion of individual heavy-fuel droplets within a two-consecutive discs' section is considered (see figure 1). This was found as the sole way to obtain the desired outputs (Plat, 1994; Di Pretoro and Manenti, 2020; Greenspan, 1983). Precisely, motion equations of the denser droplets are computed as time equations found within the literature are in disagreement (Plat, 1994) or studies on centrifuge are not entirely representative of this case (Plat, 1994; Schaflinger and Stibi, 1987; Schaflinger et al., 1986; Ungarish, 1989; Perazzolo Disconzi and Torres Borghi, 2020). From the motion equations it is possible to calculate the separation time and plot the denser droplets trajectory to assess the centrifuge performance.
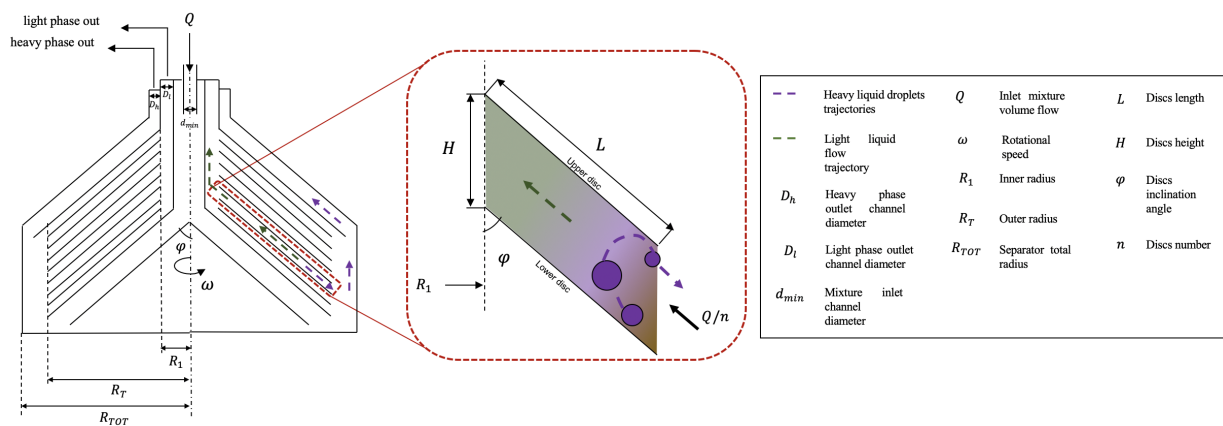


Figure 1: Disc-stack centrifuge (left) and view of two-consecutive-disc section (right), adapted from (B. Vermeire, 2021; Plat, 1994; Di Pretoro and Manenti, 2020).

The motion equations are built by computing the drag, buoyancy and centrifugal forces exerted on the denser droplets (Greenspan, 1983). Other forces are present but they are negligible compared to the centrifugal force (Plat, 1994). The model is built around the following assumptions:

- Binary mixture: HVO and methanol are the only mixture's constituents.

Figure 2: Fuels' trajectories within two-consecutive-disc section and forces on the heavy-fuel droplet.

- Ideal separation: the outlet flow equals the inlet throughput.

- The denser droplet maintains a perfect spherical shape and constant size from inlet to outlet conditions. This assumption follows the hypothesis of negligible shear stress.

- The flow through the discs' section is uniform. This stems from neglecting droplets break-up as the motion is representative of a single droplet.
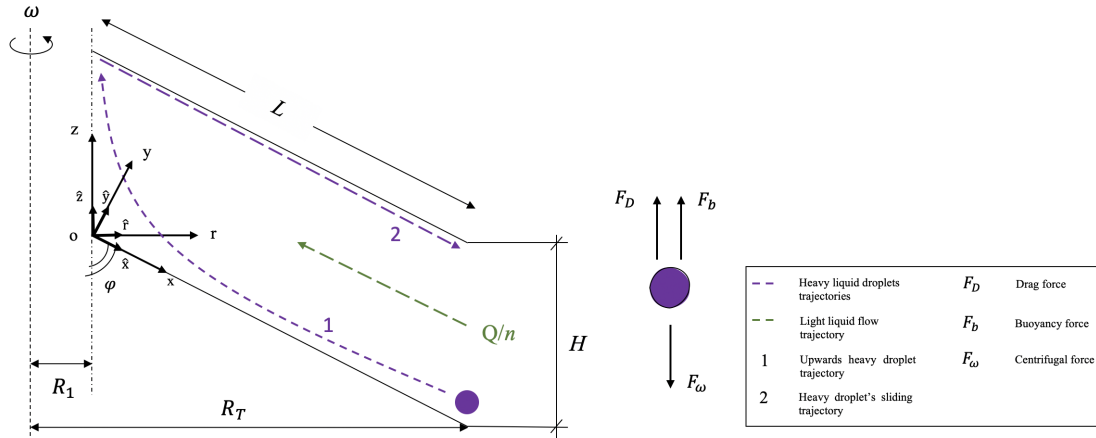
- When the droplets hit the upper disc they slide along it without friction.

The motion equations are derived by constraining the two-dimensional spacial domain to a two-consecutive-disc section and for the reference frame of figure 2. The dispersed droplets enter the discs' section travelling a certain distance before hitting the upper disc. Here, they coalesce towards the outer wall getting discharged (Di Pretoro and Manenti, 2020; Plat, 1994). Derivation of the equations is given in appendix A.1. The obtained motion equations are:

$$\ddot{x} = \frac{\pi}{6} \frac{D_p{}^3 \Delta\rho}{m_d} (x\,sin\varphi + y\,cos\varphi)\omega^2 sin\varphi - \frac{N}{m_d}(\dot{x} + V_F) \tag{1}$$

$$\ddot{y} = \frac{\pi}{6} \frac{D_p{}^3 \Delta\rho}{m_d} (x\,sin\varphi + y\,cos\varphi)\omega^2 cos\varphi - \frac{N}{m_d}\dot{y} \tag{2}$$

Explanation of terms as in appendix A and figure 1. $N$ is a function of Reynolds number:

$$N = \begin{cases} -3\pi\mu_l D_p & Re < 1 \\ \left(\frac{3\pi\mu_l D_p}{\dot{x}+V_F} + \frac{9}{16}\pi\rho_l D_p{}^2\right)\cdot & 1 \leq Re < 5 \\ \quad \cdot \left(\sqrt{(\dot{x}+V_F)^2 + \dot{y}^2}\right) & \\ \frac{\pi}{8}\rho_l D_p{}^2 \cdot 1.85\cdot & 5 \leq Re < 5000 \\ \quad \cdot \left(\frac{\rho_l D_p}{\mu_l}(\dot{x}+V_F)\right)^{-0.6} & \end{cases} \tag{3}$$

Regarding the interface, its correct allocation inside the disc-bowl, is a supplementary method to assess the centrifuge performance alongside the denser droplets' motion. This because equations 1 and 2 depend on the droplet's diameter, whose exact value is hard to determine in a liquid mixture. The interface is a section formed by the two liquids. Its correct allocation ensures no mutual liquids' contamination (B. Vermeire, 2021). There are contrasting viewpoints for siting this demarcation (Ambler, 1952; B. Vermeire, 2021; van der Linden, 1987). Overall, the interface shall be as close as possible to the disc periphery ($x = L$, see Figure 2) (GEA Westfalia, n.a.b), with equation stemming from the pressure difference at this boundary (Di Pretoro and Manenti, 2020):

$$R_{int} = \sqrt{R_T^2 + \frac{\rho_l}{\rho_h}\left(\frac{Q_l^2}{S_l^2\omega^2}\right) - \frac{Q_h^2}{S_h^2\omega^2}} \tag{4}$$

$Q_l$ and $Q_h$ are the discharged flows of the light and heavy liquid respectively, which, for an ideal separation stem from the relative concentrations in the fed mixture $X_l$ and $X_h$:

$$Q_l = X_l \cdot Q \tag{5}$$

$$Q_h = X_h \cdot Q \tag{6}$$

Assumed methanol volume in the mixture is 10%, based on (GEA Westfalia Separator Group GmbH, n.a.). Moreover, in equation 4, $S_l$ and $S_h$ are the outlet sections of the light and heavy phase respectively (Di Pretoro and Manenti, 2020).

### 2.2.2 Centrifugal model input

Equations 1, 2 and 4 to assess the centrifuge performance depend on the centrifuge inlet flow. This is derived by the HVO/methanol flows required in single- and dual-fuel engine modes, computed from the shaft power (Woud and Stapersma, 2003). The inlet centrifuge's flow is determined from equations 5 and 6. In single (SF)- and dual fuel (DF) modes it equals:

$$Q_{sep,SF} = \frac{Q_{HVO,eng,max}}{X_{HVO}} \tag{7}$$

$$Q_{sep,DF} = \frac{Q_{MeOH,eng,max}}{X_{MeOH}} \tag{8}$$

Where $Q_{MeOH,eng,max}$ and $Q_{HVO,eng,max}$ respectively are the maximum methanol and HVO volume flows demanded by the gensets. More details in (La Colla, 2023). Operations on multiple fuels yield different HVO-methanol mixtures in the storage tanks during bunkering. The studied cases comprise:

- Single-fuel (HVO) engine mode: bunkered HVO with residual methanol in the storage tanks at 5% v/v.

- Dual-fuel (HVO-methanol) engine mode: bunkered methanol with residual HVO in the storage tanks at 5% v/v.

Additional assumptions are:

- Dedicated service tanks as to SOLAS (IMO, 2018).

- Both methanol and HVO service tanks full at bunkering.

- The mixture fed to the separator consists of methanol-HVO at 10-90% v/v. This ratio is kept constant as based on (GEA Westfalia Separator Group GmbH, n.a.).

### 2.2.3 Centrifuge performance assessment and sizing

The study aims at finding a separator design guaranteeing complete fuels' separation in both SF and DF engine modes. Iteration through the motion equations 1 and 2 is followed. The minimum droplet diameter for denser droplets to separate, coalescing towards the heavy-phase outlet, is determined by varying the rotational speed. Additionally, a single-objective optimization finds the optimal combinations of the centrifuge design parameters satisfying:

$$0.7 \cdot L \le min\ f \le 0.3 \tag{9}$$

With:

$$f = \frac{\frac{R_{int}}{sin\varphi} - L}{\frac{R_T}{sin\varphi} - L} \tag{10}$$

And $R_{int}$ calculated as in equation 4, while equation 9 defines an acceptable interface position range given a limited quantitative definition of its ideal location within the literature. Furthermore, referring to figure 1, the separator total diameter equals:

$$D_{TOT} = 2 \cdot \left( \frac{D_l}{2} + R_T \right) \tag{11}$$

*2.2.4   Spin tests*

Spin tests were conducted to validate the mathematical model. They are the first industrial step to predict a centrifuge performance (SEPARATECH, n.a.). Liquid-filled spin tubes are placed in a bench-top machine, applying centrifugal force to the mixtures at specified temperature and time.

Tests were conducted on HVO and methanol mixtures with respectively a density of 771 and 793 kg/m$^3$ at 20°C. The fuels were poured in glass tubes and mixed manually. Subsequently, the mixture was poured in spin tubes for centrifugation within 30-40 seconds. The mixture's total volume equals 10 ml and tests were performed on methanol at 2 and 98% v/v. The mixtures were centrifuged in the spin machine for 4, 8 and 16 minutes at 20°C and 2100 rpm.

## 3   Results

Results are presented for the phase separation experiments, the centrifuge mathematical model and the spin tests.

### 3.1   Gravity separation

The results of the gravity separation experiments are shown in figure 3. Overall, bigger droplets settled faster, confirming an inverse relationship between settling time and droplet's diameter (De Haan et al., 2020; Ishii and Zuber, 1979; Richardson and Zaki, 1954). The microscope showed methanol droplets in HVO for all mixtures and time intervals. A result confirmed by the cloudy appearance of all mixtures. Different behaviours were observed with varying methanol concentrations and a correlation was found between the separation time and the methanol droplets' diameter. In figure 3, results are shown for methanol at 5-70% v/v at the time intervals at which the liquid samples were extracted from the beaker. The average methanol droplets' diameter and associated standard error are indicated.
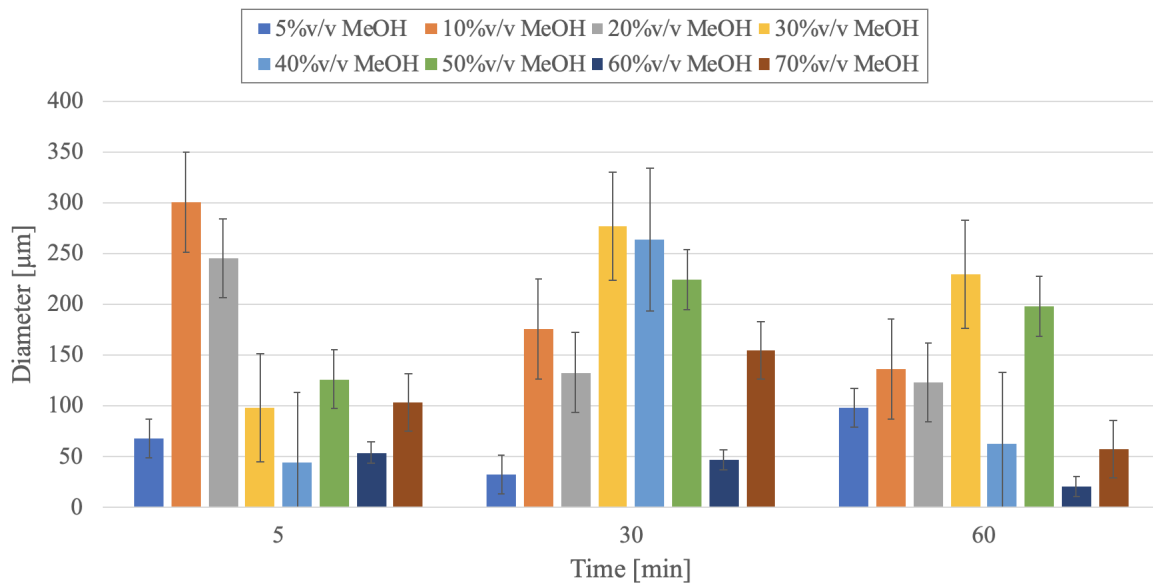


Figure 3: Average diameter of methanol droplets for different methanol concentrations.

For methanol at 5-20% v/v, figure 3 shows droplets size decreasing after 30 minutes compared to the 5-minute case. Larger droplets settled within 30 minutes, while smaller droplets persisted in the beaker column due to the relatively low methanol ratio, which inhibited coalescence by maintaining small inter-droplet distances. Droplets' conjunction occurred after 1 hour for methanol at 5% v/v. Nevertheless, this is not the case for 10-20% volumes. Precisely, after 1 hour methanol droplets remained smaller compared to the 30-minute observation. It is hypothesized that the droplets already merged between 30 and 60 minutes, leaving only the tiny droplets in the HVO column.

For methanol at 30-50% v/v droplets increased after 30 minutes and reduced after 60 minutes. Larger droplets settled faster leaving the smaller droplets behind, thus explaining the relatively small diameters after 5 minutes. Subsequently, these small droplets merged after 30 minutes, forming bigger ones. The size decrease became less pronounced with methanol at 50% v/v.

For methanol at 60-70% v/v. with methanol as the continuous phase, droplets displayed a different behaviour. For 60% v/v methanol, coalescence is faster because methanol droplets after 30 and 60 minutes are smaller than the

first observation. This could be explained by the higher HVO dynamic viscosity compared to methanol. In fact, a lower viscosity of the continuous phase accelerates coalescence, hence droplets settling (Jeffreys and Davies, 1971). Thus, the methanol droplets already merged and coalesced in the 5-30 minute interval. This trend continues after 30 minutes, with the methanol droplets becoming even smaller. Conversely, for methanol at 70% v/v, droplets increase in size only after 30 minutes, indicating a longer merging time compared to the 60% v/v case.

Samples with methanol at 1 and 50% v/v were inspected after three days. The droplets became tinier than in all shown cases, especially for methanol at 50% v/v. Observed methanol in HVO after three days indicates that full separation does not happen within three days, due to the low-density difference between the fuels (see Table 1) and the dynamic viscosity of both substances (Green and Perry, 2008). Conversely, partial separation may result from the different fuels' polarity (Roberts et al., 1971; Neste, 2020; Lapuerta et al., 2015).

Lastly, a test was performed by doubling the mixture's total volume with methanol at 30% v/v, showing methanol droplets size decreasing, particularly after 1 hour. This result can extend the time required for full separation onboard yachts, as the gravity-settling tanks' capacity is significantly larger than the tested mixture's total volume.

Consequently, all the tested mixtures failed to achieve full separation in the 1 hour-3 day time-frame, rendering the use of gravity-settling tanks onboard impractical for quasi-instantaneous clean fuel supply to converters.

### 3.2 Centrifugal separation

This section presents the results of the centrifuge mathematical model and spin tests.

#### 3.2.1 Mathematical model

Results are presented for the centrifuge's dimensions and the droplets' motion.

- **Interface position**: to iteratively meet the condition in equation 9, a first set of input design values is given to the model based on (McGeorge, 1998; Plat, 1994; Di Pretoro and Manenti, 2020; van der Linden, 1987; GEA Westfalia, n.a.b; Alfa Laval, n.a.). The results are depicted in Figure 4 and shown for the single- and dual-fuel yacht's modes, i.e. respectively for the separator inlet flows $Q_{sep,SF}$ and $Q_{sep,DF}$.
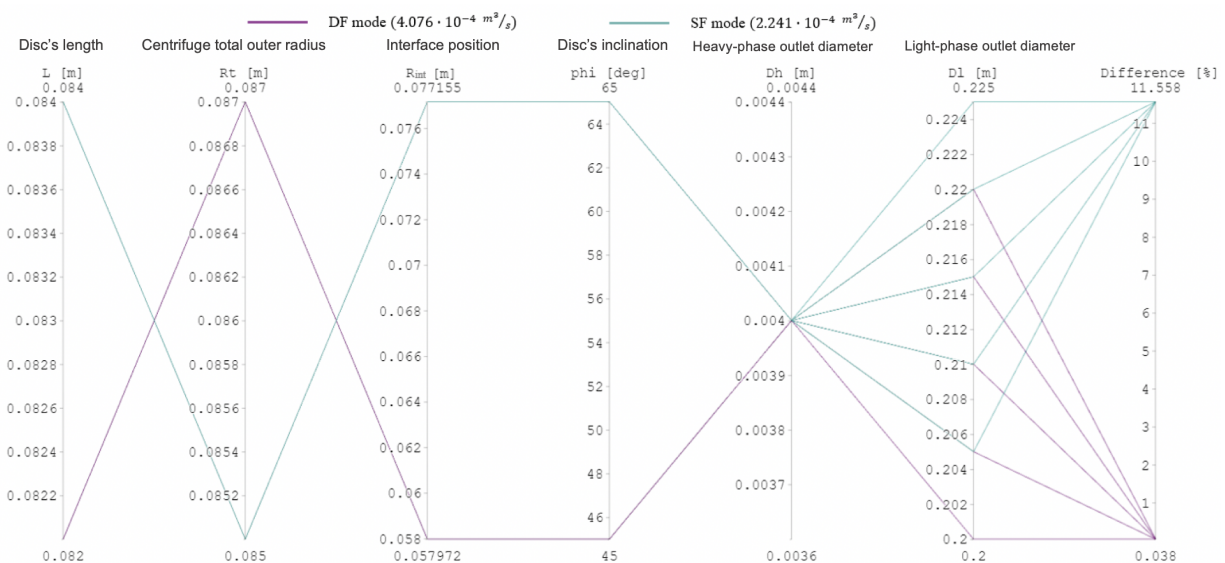


Figure 4: Five best combinations of centrifuge design parameters for optimal interface position. Results from last iteration process for dual- and single-fuel engine modes.

Across iterations, discs' length values neared the highest in the range, whilst the total centrifuge's radius ($R_T$) scored the lowest, due to the small values added to $R_T$ as in equation 4. Given similar densities, $\rho_l/\rho_h \approx 1$, hence the $R_{int}$ variation is dictated by volume flow, outlet sections diameter and rotational speed. Concerning the volume flow, the plot depicts minimal variation among input values. However, the percentage difference is lower in the dual-fuel mode case, particularly at higher volume flows. This may be due to pressure difference variation at the interface and higher mixture flow velocity entering the separator, dragging dispersed droplets towards the discs' section rather than the outer wall, as shown in equation 17. However, although the volume flow is varied to simulate the two engine modes, the assumed value is a constant within the separator design. Hence, $\omega$, $D_h$ and $D_l$ are the parameters varying the added terms to $R_T$ in

equation 4. Nevertheless, the rotational speed is constant within the iterations. Hence, regarding the outlet sections' diameter, for heavy phase at fixed 10% v/v, $Q_l > Q_h$. Moreover, $D_l > D_h$ in existing separators, compensating for the difference between $Q_l$ and $Q_h$. Consequently, given two fuels with close densities, the value of $R_{int}$ strictly depends on the discs' length and the total outer radius.

- **Droplets' trajectory**: The results of the separator specification are used as inputs for the iteration on the motion equations 1, 2. Results are depicted in Figures 5 to 8 for single- and dual-fuel yacht's modes, i.e. at a centrifuge inlet flow of respectively $2.241 \cdot 10^{-4}$ and $4.076 \cdot 10^{-4}$ m$^3$/s. The droplets' trajectories are plotted for droplet's diameter ($D_p$) of 5-100 $\mu m$ as found in (Frising et al., 2008; Plat, 1994). The graphs portray the methanol (heavy-phase) droplets' trajectories within a separator discs' section.
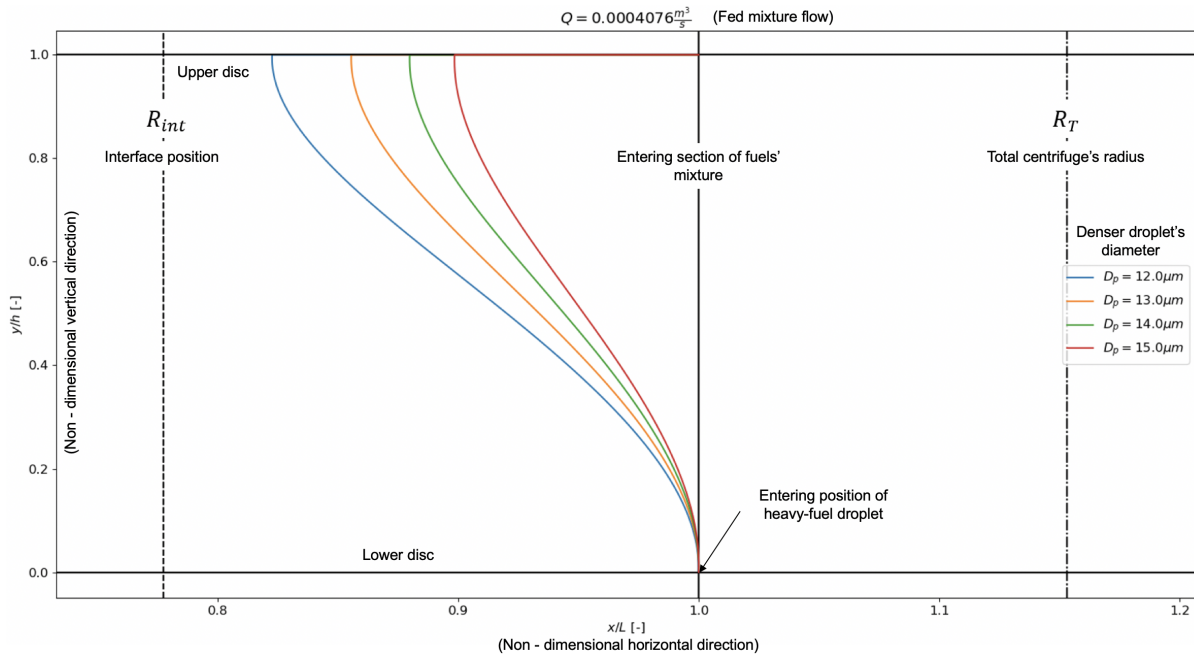


Figure 5: Trajectories of medium-sized methanol droplets within two-consecutive-disc section (dual-fuel engine mode).
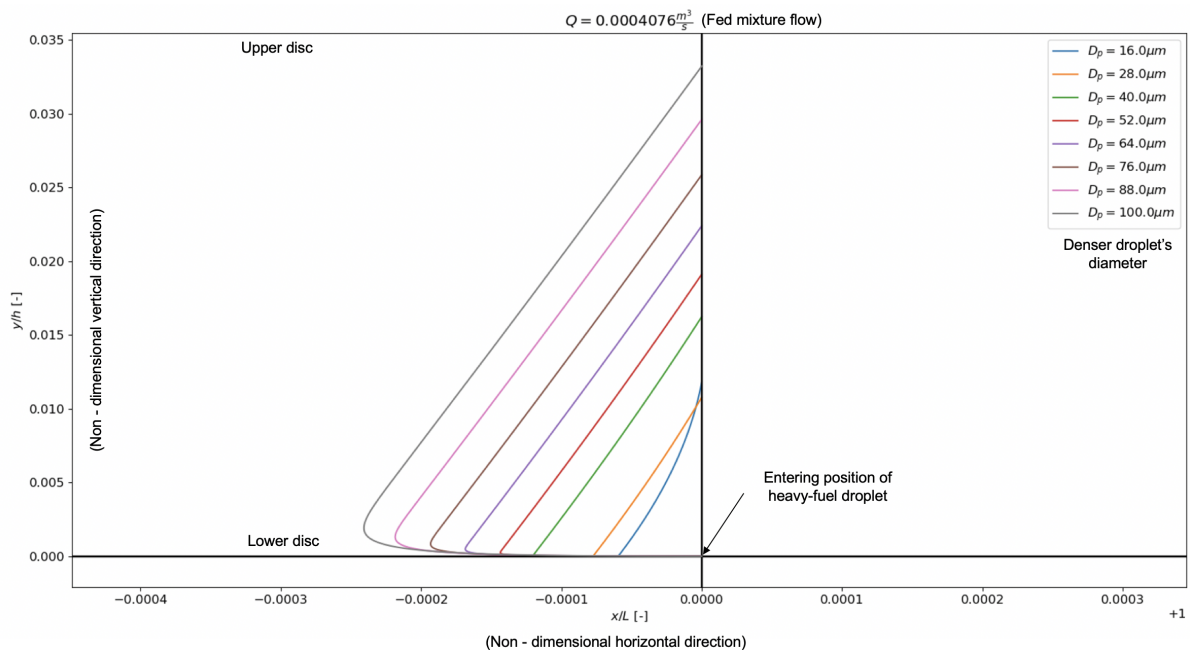


Figure 6: Trajectories of big-sized methanol droplets within two-consecutive-disc section (dual-fuel engine mode).
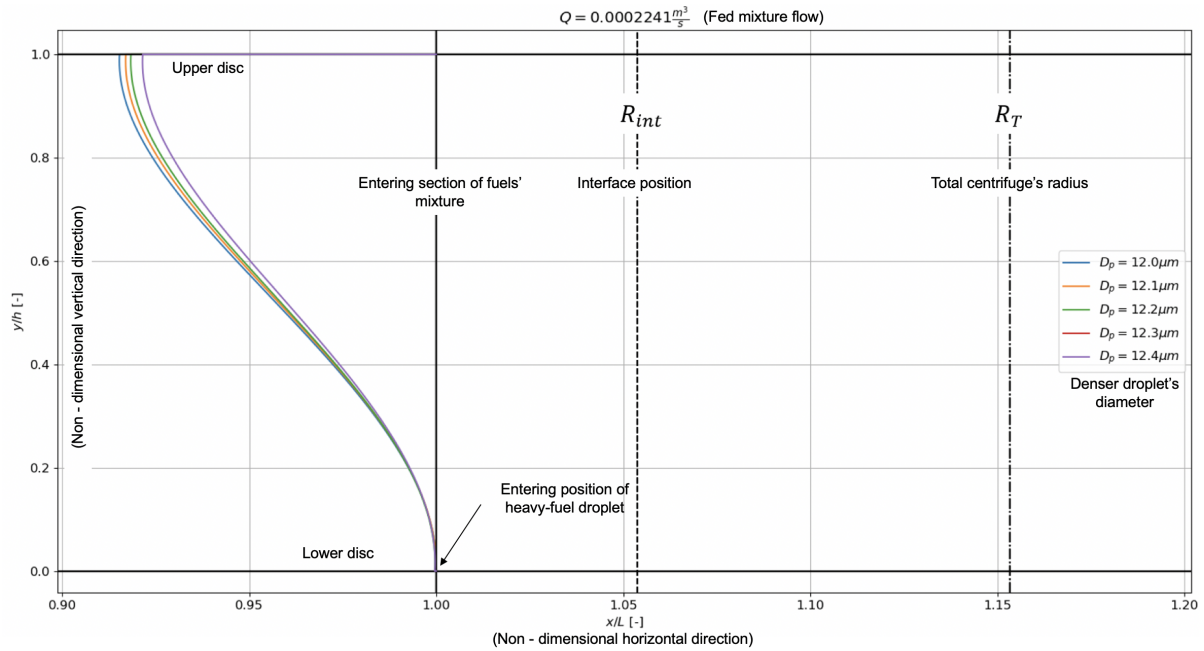
Figure 7: Trajectories of medium-sized methanol droplets within two-consecutive-disc section (single-fuel engine mode).
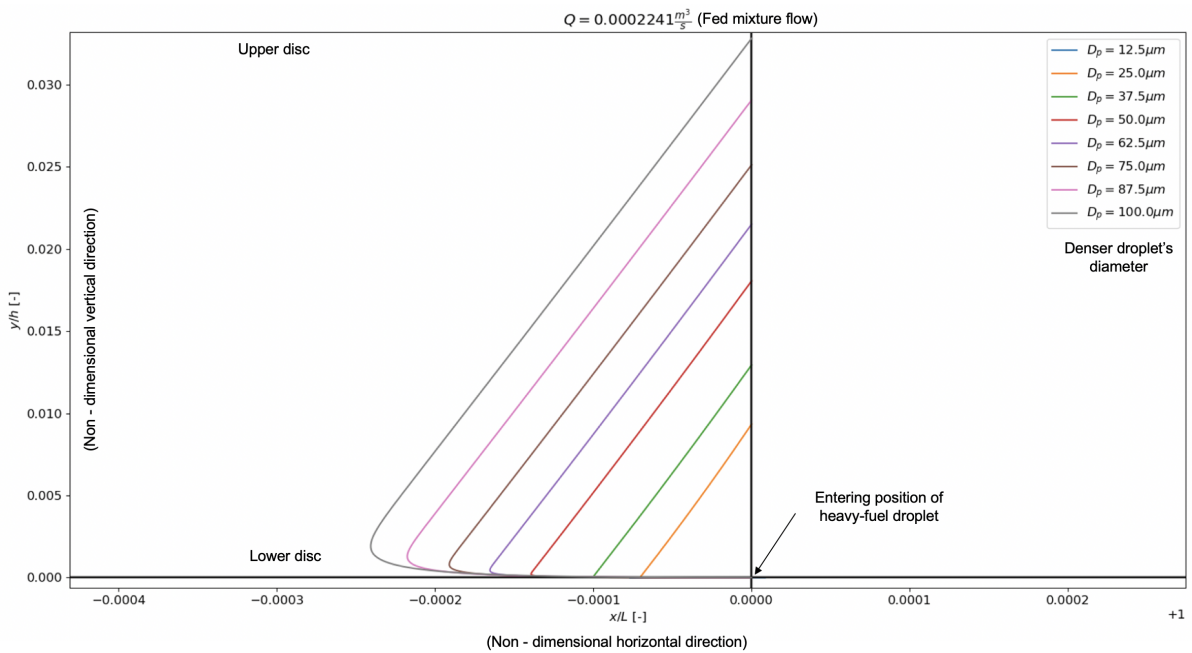


Figure 8: Trajectories of big-sized methanol droplets within two-consecutive-disc section (single-fuel engine mode).

In all plots droplets coalescence towards the heavy-phase outlet. Thus, with the found separator design, full separation is achieved. Droplets with diameters smaller than the presented values also get discharged in the methanol outlet. Their trajectories are not shown here for graph's readability and due to negligible differences found between the studied operational modes.

Figures 5 and 7 show the trajectories for droplets with diameter from 12-15 $\mu$m. For a higher flow, the travelled distance by the droplets is bigger compared to a lower flow, due to greater velocity of the single droplet. Furthermore, the travelled distance rises the smaller the droplet, yielding the assumption that smaller droplets show less resistance to the fed mixture's flow. Additionally, for a higher flow, the interface ($R_{int}$)

falls inside the discs' section, whilst it allocates outside for a lower flow. Hence, for higher flows the denser droplets are dragged more towards the discs' section rather than the outer wall.

Regarding bigger droplets, figures 6 and 8 show no major differences between the two operational modes. All droplets leave the discs' section quasi-instantaneously, assuming centrifugal force dominating over drag. For higher flows the droplets travel a bigger distance compared to lower flows. However, this difference is slighter than the medium-sized droplets' case.

Lastly, the resulting separation time is discussed. For continuously-operating centrifuges, this is dictated by the denser droplets' coalescence time. Droplets sized 16-100 $\mu$m in diameter get discharged in few milliseconds. Droplets sized 12-15 $\mu$m coalesce within some minutes. Specifically, their velocity is dominated by the entering mixture's velocity, thus the droplets require some seconds to move upwards and hit the upper disc. Here, kinetic energy is lost (Di Pretoro and Manenti, 2020), thus the droplet needs to overcome the incoming mixture's resistance when flowing towards the methanol outlet section. The demanded time increases the lower the droplet's diameter. The 12 $\mu m$ sized droplets need around 10 minutes to get discharged in dual-fuel mode. In single-fuel engine mode, when the separator-fed volume flow is lower, the discharged time is also lower, accounting for about 5 minutes.

The final centrifugal separators' specifications are listed in Table 2.

Table 2: Final specifications of the modelled centrifugal separator

| Parameter | Symbol | Unit | Value |
|---|---|---|---|
| Fed mixture volume flow (DF mode) | $Q_{sep,DF}$ | [m$^3$/s] | $4.076 \cdot 10^{-4}$ |
| Fed mixture volume flow (SF mode) | $Q_{sep,SF}$ | [m$^3$/s] | $2.241 \cdot 10^{-4}$ |
| Discs' length | $L$ | [m] | 0.084 |
| Methanol outlet section diameter | $D_h$ | [m] | 0.004 |
| HVO outlet section diameter | $D_l$ | [m] | 0.205 |
| Separator total diameter | $D_{TOT}$ | [m] | 0.379 |
| Rotational speed | $\omega$ | [rad/s] | 50 |

### 3.2.2 Spin tests

HVO-methanol mixtures separation at 98-2 and 2-98 % v/v was tested in a spin machine. It resulted that both mixtures failed at achieving full separation.

For the case of HVO-methanol at 98-2 % v/v, 0.5% v/v methanol coalesced to the bottom of the test tube after 4 minutes. Nevertheless, no further improvement resulted when increasing spin time to 8 and 16 minutes.

Regarding HVO-methanol mixture at 2-98% v/v, traces of HVO were observed at the top of the tube after 4 minutes. Similar result occurred after 8 and 16 minutes, accounting for approximately 0.2% v/v emulsion.

Full separation was not achieved under the tested conditions. A volume percentage, relative to the dispersed fuel, was present in the continuous liquid for all mixtures. This suggests a dilution of the residual fuel in the bunkered fuel, which cannot be separated using the applied methodology.

### 3.2.3 Results validation

The validity of the centrifugal separation mathematical model and spin tests are scrutinized in this subsection. Evaluation of the model's hypotheses is performed showing consistency with the results (see appendix B). Below the mathematical model results are compared with literature findings and a comparison is conducted between the model and the spin test results.

- **Validation of centrifuge's dimensions**: the centrifuge's results of Table 2 are scrutinized to ascertain the model's validity.

A centrifuge by *Alfa Laval* (Alfa Laval, n.a.) works at 71.7 rad/s, faster than 50 rad/s obtained in this study due to the higher separator capacity. The *Alfa Laval* design works at a 35-64 times higher flow than the one in this case. Hence, a higher rotation efficiently allocates the liquids' interface. Furthermore, density difference of separated compounds in the manufacturer's separator is larger than the HVO-methanol case

(ECHA, n.a.). Similarly, due to the interface allocation, the manufacturer's design presents a heavy-phase outlet diameter larger than the result here obtained. Same discussion applies to the tested oil-water separator by (van der Linden, 1987) at a rotation of 91.7 rad/s. The design by (Plat, 1994) leads to similar conclusions, where the discs' length and the separator radius are respectively 16.7% and 47.2% smaller than the obtained values. This can still be due to the higher density difference between the tested oil and water by (Plat, 1994) compared to the HVO-methanol case. The resulting centrifuge diameter is 34.9% bigger than the maximum diameter of separators in yachts (GEA Westfalia, n.a.a). Likewise, the cause can be the lower density difference between HVO and methanol compared to the diesel-water case of marine separators. The centrifuge diameter is, in fact, influenced by the HVO outlet diameter, as evident from Table 2, aligning with the recommendations from (GEA Westfalia, n.a.b).

Moreover, the calculated starting time is 5-10 minutes depending on the separator inlet flow. The already mentioned centrifuges report 2-4 (GEA Westfalia, n.a.b) and 6-8 minutes (Alfa Laval, n.a.) starting time. Nevertheless, it is unclear if this time only comprises droplets' coalescence or it includes other processes, namely ramp-up.

- **Mathematical model - validation**: the results of the centrifuge's model and spin tests are discussed for comparison. The model showed achievable full separation with a larger separator compared to existing designs. Conversely, the tests evidenced incomplete separation. This deriving from the dilution of the residual fuel in the bunkered one. An effect possibly stemming from forces exerted on the fuels and the velocity of the dispersed droplets while mixing, which could have affected the droplets' size (Coulaloglou and Tavlarides, 1977; Howarth, 1964; Sovová, 1981). In fact, as subsection 3.1 reported, the droplets' size determines the dispersed liquid's coalescence. The dilution phenomenon was not integrated in the mathematical model, which limits to describe the individual denser droplet's motion by neglecting the droplets relative interference. This derives from neglected shear forces. These phenomena can occur in storage tanks, however they are hard to predict.

Additionally, the spin tests were conducted with the dispersed phase at 2% v/v whilst a 10% v/v was assumed in the mathematical model. The dispersed liquid's concentration can affect the mixture's status (Privat et al., 2013).

Furthermore, in a disc-stack centrifuge, the heavy-droplet's dynamics differ from spin tests. Droplets move between two consecutive discs, separating upon impact with the upper disc or if deviating towards the desired outlet. Among influencing parameters, the fed mixture flow affects droplet behavior and interface position variation. Conversely, in spin tubes, droplets move within a disc-free cylindrical space, independent of inlet flow. Additionally, no interface position is identifiable, thus not accounting for pressure balance.

Consequently, the mathematical model and spin tests yield differing results due to the dilution effect of residual fuel and the spatial domain of dispersed droplets. The model accurately simulates the dynamics of individual dispersed droplets within the centrifuge's discs. Conversely, spin tests offer insights into potential dilution effects in storage tanks or during centrifugation.

## 4 Conclusions and further research

This work explored separation of HVO-methanol mixtures, given concerns about mutual contamination in dual-fuel engines and fuel cells, and lack of fuels standards and research.

For separation, gravity-settling tanks and disc-bowl centrifuges were researched. Phase separation tests on HVO-methanol mixtures revealed incomplete separation within 1 hour-3-day time-frame due to the low-density difference between the fuels, rendering gravity-settling tanks impractical for use onboard.

Regarding centrifuges, a mathematical model was computed to observe denser droplets' trajectory within the discs' interspace and the interface position's variations. A centrifuge design enabling full separation per engine mode was defined. Moreover, spin tests were conducted for model's validation.

The model suggests achieving full fuels separation with a disk-stacked centrifuge 34.9% larger in diameter than typical separators onboard yachts, due to the low-density difference between HVO and methanol. Furthermore, the maximum startup time ranges 5-10 minutes for droplets of 12-16 $\mu$m in diameter.

Droplets break-up and merge were identified as causes of the different results in spin tests where HVO-methanol mixtures partially separated, due to full liquids' dilution. This could be attributed to forces on dispersed droplets affecting coalescence. Additionally, the different results between the mathematical model and spin tests can lie in the different spacial domain of the dispersed droplets. The model remains valid for individual dispersed droplets' motion within centrifuge discs' sections. Conversely, spin tests provides insights into possible dilution, occurring in storage tanks, piping or during centrifugation.

For future work:

- Quantification of contaminants' limits of combusted fuels per technology type is suggested. Dual-fuel engines and fuel cells are recommended to be tested with HVO and methanol mutually contaminated.

- For efficient fuels treatment onboard, research into precise mixture concentration detection along the onboard converters' supply path is suggested. In gravity tests, in fact, quantifying the separated mixture over time proved unfeasible. Moreover, investigation on separation time reduction is recommended by altering stirring time and rotation in gravity tests. Here, in fact, these parameters were kept constant but can impact the dispersed droplets' size and thus the separation time.

- Investigation on centrifugal separation time and droplets' motion is suggested by including the disregarded Coriolis effects and droplet break-up and merge in the mathematical model.

- Exploration on various fuel concentrations and $\leq 7\%$ v/v FAME in HVO is suggested, as per standards (Neste, 2020). Different concentrations and FAME addition may affect the compounds' solubility and therefore the fuels' separation.

**Acknowledgement**

**References**

Alfa Laval, n.a. High-capacity disc stack centrifuge for biodiesel production. `https://www.alfalaval.com/globalassets/documents/products/separation/centrifugal-separators/disc-stack-separators/bd_95.pdf`.

Ambler, C., 1952. The evaluation of centrifuge performance. Chemical Engineering Progress 48, 150–158.

B. Vermeire, M., 2021. Everything you need to know about marine fuels. Ghent, Belgium.

Brennen, C.E., 2005. Fundamentals of multiphase flow.

Cheung, C.S., Zhang, Z.H., Chan, T.L., Yao, C., 2009. Investigation on the effect of port-injected methanol on the performance and emissions of a diesel engine at different engine speeds. Energy Fuels 23, 5684–5694. doi:`https://doi.org/10.1021/ef9005516`.

Coulaloglou, C.A., Tavlarides, L.L., 1977. Description of interaction processes in agitated liquid-liquid dispersions. Chemical Engineering Science 32, 1289–1297. doi:`https://doi.org/10.1016/0009-2509(77)85023-9`.

De Haan, A., Eral, H.B., Schuur, B., 2020. Industrial Separation Processes: Fundamentals. Boston: De Gruyter, Berlin. URL: `https://doi.org/10.1515/9783110654806`.

Di Pretoro, A., Manenti, F., 2020. Non-conventional Unit Operations: Solving Practical Issues. PoliMI Springer-Briefs, Gewerbestrasse 11, 6330 Cham, Switzerland. URL: `https://doi.org/10.1007/978-3-030-34572-3`.

Dolphin Centrifuge, 2020. Disadvantages of a disc-stack centrifuge — illustrated guide. `https://dolphincentrifuge.com/disadvantages-disc-stack-centrifuge/`.

ECHA, n.a. Chemicals regulated substances. `https://www.echa.europa.eu/`.

Ellis, J., Tanneberger, K., 2015. Study on the use of ethyl and methyl alcohol as alternative fuels in shipping. EMSA, SSPA.

Estefan, R.M., Brown, J.G., 1990. Evaluation of possible methanol fuel additives for reducing engine wear and/or corrosion. Section 4: JOURNAL OF FUELS & LUBRICANTS 99, 942–964. doi:`https://doi.org/10.4271/902153`.

European Commission, n.a. Reducing emissions from the shipping sector. `https://ec.europa.eu/clima/eu-action/transport-emissions/reducing-emissions-shipping-sector`.

Flottweg SE, n.a. Flottweg separation technology for the production of biodiesel. Technical Report. Flottweg SE.

Frising, T., Noïk, C., Dalmazzone, C., Peysson, Y., Palermo, T., 2008. Contribution of the sedimentation and coalescence mechanisms to the separation of concentrated water-in-oil emulsions. Journal of Dispersion Science and Technology 29, 827–834. doi:`10.1080/01932690701781501`.

GEA Westfalia, n.a.a. GEA Westfalia Separator OTC 2-02-137/OTC 3-02-137. Technical Data: Continuous treatment of fuel and lube oils, hydraulic, diesel, turbine and waste oils. Technical Report. GEA Westfalia.

GEA Westfalia, n.a.b. Westfalia Separator Mineraloil Systems GmbH. Technical Report. GEA Westfalia.

GEA Westfalia Separator Group GmbH, n.a. Marine system technology: Concepts and high performance equipment for the engine room gea westfalia separator. .

Green, D.W., Perry, R.H., 2008. Perry's Chemical Engineers' Handbook. 8 ed., McGraw-Hill.

Greenspan, H., 1983. On centrifugal separation of a mixture. Journal of Fluid Mechanics 127, 91–101. doi:`https://doi.org/10.1017/S0022112083002633`.

Hazar, H., Temizer, I., 2012. The engine performance of a diesel engine and the research of the effect of fuel additives on engine oil and engine parts. Scientific Bulletin of the "Petru Maior" University of Tîrgu Mureș 9(XXVI), 50–57. URL: `http://scientificbulletin.upm.ro/`.

Howarth, W.J., 1964. Coalescence of drops in a turbulent flow field. Chemical Engineering Science 19, 33–38. doi:`https://doi.org/10.1016/0009-2509(64)85003-X`.

IMO, 2018. Solas 2018 - consolidated edition. .

IMO, 2022. Report of the Marine Environment Protection Committee on its seventy-eight session. `https://www.imo.org/en/MediaCentre/MeetingSummaries/Pages/MEPC-78th-session.aspxx`.

IMO, 2023. Revised ghg reduction strategy for global shipping adopted. `https://www.imo.org/en/MediaCentre/PressBriefings/Pages/Revised-GHG-reduction-strategy-for-global-shipping-adopted-.aspx`.

Ishii, M., Zuber, N., 1979. Drag coefficient and relative velocity in bubbly, droplet or particulate flows. Aiche Journal 25, 843–855. doi:`https://doi.org/10.1002/aic.690250513`.

Jeffreys, G.V., Davies, G.A., 1971. Chapter 14 - coalescence of liquid droplets and liquid dispersion. Recent Advances in Liquid–Liquid Extraction , 495–584doi:`https://doi.org/10.1016/B978-0-08-015682-8.50018-3`.

Kamp, J., Villwock, J., Kraume, M., 2016. Drop coalescence in technical liquid/liquid applications: a review on experimental techniques and modeling approaches. Reviews in Chemical Engineering doi:`https://doi.org/10.1515/revce-2015-0071`.

Kato, M., Muramatsu, T., Tanaka, H., Moriya, S., Yaginuma, F., Isshiki, N., 1991. Density behavior of alcohol-diesel fuel mixtures. Journal of The Japan Petroleum Institute 34, 186–190.

Kerr, R.M., 2007. Biodiesel Production Techniques. Technical Report.

Kries, M.J., 2021. A Methanol impact tool for yachts, assessing the impact of using methanol as an alternative fuel on the design, emissions and costs of yachts. Master's thesis. Delft University of Technology.

La Colla, E., 2023. Experimental and modelling studies on HVO-methanol mixtures separation for superyachts applications. Master's thesis. Delft University of Technology.

Lambregts, T., 2021. Fuel-Flexibility, Fuel-flexible fuel cell systems for super yachts. Master's thesis. Delft University of Technology.

Lapuerta, M., Rodríguez-Fernandez, J., García-Contreras, R., Bogarra, M., 2015. Molecular interactions in blends of alcohols with diesel fuels: Effect on stability and distillation. Fuel 139, 171–179. doi:`https://doi.org/10.1016/j.fuel.2014.08.055`.

van der Linden, J., 1987. Liquid-liquid separation in Disc-Stack Centrifuges. TR Diss 1525, Delft University of Technology.

McGeorge, H.D., 1998. Marine Auxiliary Machinery. Elsevier, Oxford.

Nautiyal, P., Gondal, A., Kumar, D., 1989. Wear and lubrication characteristics of a methanol-fuelled compression ignition engine — a comparison with pure diesel and bifuel operation. Wear 135, 67–78. URL: `https://doi.org/10.1016/0043-1648(89)90096-3`.

Neste, 2020. Neste Renewable Diesel Handbook. Technical Report.

Perazzolo Disconzi, F., Torres Borghi, F., 2020. Modeling, simulation, and optimization of the centrifugal separation of a microalgae-culture medium mixture. Biomass and Bioenergy 143. doi:`https://doi.org/10.1016/j.biombioe.2020.105871`.

Plat, R., 1994. Gravitational and centrifugal oil-water separators with plate pack internals. Delft University of Technology.

Privat, R., Jaubert, J.N., Molière, M., 2013. The thermodynamics of alcohols-hydrocarbons mixtures. MATEC Web of Conferences 3, 01018. doi:`https://doi.org/10.1051/matecconf/20130301018`.

Richardson, J., Zaki, W., 1954. The sedimentation of a suspension of uniform spheres under conditions of viscous flow. Chemical Engineering Science 3, 65–73. doi:`https://doi.org/10.1016/0009-2509(54)85015-9`.

Roberts, J.D., Stewart, R., Caserio, M.C., 1971. Organic chemistry: Methane to macromolecules. W. A. Benjamin, INC., New York.

Schaflinger, U., Köppl, A., Filipczak, G., 1986. Sedimentation in cylindrical centrifuges with compartments. Ing. arch 56, 321–331. doi:`https://doi.org/10.1007/BF02570612`.

Schaflinger, U., Stibi, H., 1987. On centrifugal separation of suspensions in cylindrical vessels. Acta Mechanica 67, 163–181. doi:`https://doi.org/10.1007/BF01182130`.

SEPARATECH, n.a. Spin test for evaluating the centrifugation performance of centrifuge. `https://www.separatech.com/spin-test-for-evaluating-the-centrifugation-performance-of-centrifuge/`.

Siepmann, T., 2019. Integrating Large-Scale Hydrogen Storage on Superyachts: A Feasibility Analysis and Con-

cept Study. Master's thesis. Chalmers University of Technology.

Sorsamäki, L., Nappa, M., 2015. Design and selection of separation processes. Technical Report. VTT.

Sovová, H., 1981. Breakage and coalescence of drops in a batch stirred vessel—ii comparison of model and experiments. Chemical Engineering Science 39, 1567–1573. doi:`https://doi.org/10.1016/0009-2509(81)85117-2`.

Sterchi, J., 2001. The effect of hydrocarbon impurities on the methanol steam -reforming process for fuel cell applications. Master's thesis. University of Florida.

Taylor, D.A., 1996. Introduction to marine engineering. Elsevier, Oxford.

Towler, G., Sinnott, R., 2013. Chapter 16 - separation of fluids. Chemical Engineering Design (Second Edition) , 753–806doi:`https://doi.org/10.1016/B978-0-08-096659-5.00016-X`.

Ungarish, M., 1989. Side wall effects in centrifugal separation of mixtures. Physics of Fluids A: Fluid Dynamics 1, 810–818. URL: `https://doi.org/10.1063/1.857378`.

Visser, B., 2021. The Plug-in Hybrid Electric Superyacht: An operational data-driven design. Master's thesis. Delft University of Technology.

van der Vliet, N., 2021. Green Refits: Reducing yacht operational emissions through refitting. Master's thesis. Delft University of Technology.

Washecheck, P. H., Liu, A. T. C., Kennedy, E. F., 1983. Methanol fuel and methanol fuel additives. `https://patents.google.com/patent/US4375360A/en`.

Woud, H.K., Stapersma, D., 2003. Design of Propulsion and electric generation system. IMarEST - The Institute of Marine Engineering, Science and Technology, London.

## Appendix A

### *A.1 Derivation of motion equations*

The denser droplets enter the discs' section with an acceleration in the x-direction which can be decomposed as:

$$\ddot{\vec{x}}_d = \ddot{x}\hat{x} + \ddot{y}\hat{y} \tag{12}$$

This is used to express the forces balance via the Newton's second law:

$$\sum \vec{F} = m_d \ddot{\vec{x}}_d \tag{13}$$

Where $m_d$ is the heavy droplet mass proportional to the denser droplet's diameter $D_p$(De Haan et al., 2020; Plat, 1994). The forces vector is the summation of the buoyancy, centrifugal and drag forces experienced by the droplet (McGeorge, 1998; De Haan et al., 2020; Plat, 1994). Respectively:

$$\vec{F}_b = -\frac{\pi}{6}D_p{}^3\rho_h r\omega^2 \hat{r} \tag{14}$$

$$\vec{F}_\omega = \frac{\pi}{6}D_p{}^3\rho_l r\omega^2 \hat{r} \tag{15}$$

$$\vec{F}_D = C_D \frac{\pi D_p{}^2}{4}\frac{1}{2}(\vec{V}_F - \vec{V}_d) \tag{16}$$

In equation 16 $\vec{V}_F$ and $\vec{V}_d$ respectively indicate the velocity of the flow entering the single discs' section and the velocity of the denser droplet. The expression for $\vec{V}_F$ is computed from the denser droplet's initial conditions, as expressed n appendix A.2 and derived in appendix A.3. Its final expression is:

$$V_F(x,y) = \frac{3QL}{\pi nxH^2 sin^2\varphi}yL\left(1 - \frac{y}{H\,sin\varphi}\right) \tag{17}$$

The term $C_D$ in equation 16 represents the drag coefficient and it is a function of the Reynolds number (De Haan et al., 2020):

$$C_D = \begin{cases} \frac{24}{Re} & Re < 1 \\ \frac{24}{Re}(1 + \frac{3}{16}Re) & 1 \leq Re < 5 \\ 1.85Re^{-0.6} & 5 \leq Re < 5000 \end{cases} \tag{18}$$

With the Reynolds number of the droplet (Brennen, 2005):

$$Re = \frac{\rho_l D_p}{\mu_l}(\dot{x} + V_F) \tag{19}$$

By manipulating equations above, the motion equations 1 and 2 are obtained.

### A.2 Initial conditions

Initial conditions are imposed to solve the coupled second-order differential motion equations 1 and 2, and confine the spatial domain of the droplet movement within a two-successive discs' section. Referring to Figure 2, initial conditions are imposed for both trajectories 1 and 2. The subscripts $i,j$ respectively $i$ refer to the first ($i = 1$) and the second trajectory ($i = 2$). The subscript $j$ equals 0, meaning that that condition is set for the relative time $t = 0$ at which the droplet enters the section. The initial conditions for the first trajectory are:

$$\begin{cases} x_{10} = L \\ y_{10} = 0 \\ \dot{x}_{10} = \dot{x}_{10} \\ \dot{y}_{10} = 0 \end{cases} \tag{20}$$

The droplet enters at the lower disc's edge with a velocity of the fed mixture in x-direction (Di Pretoro and Manenti, 2020). This is defined by imposing the forces equilibrium along x:

$$\dot{x}_{10} = \frac{16\mu_l}{3\rho_l D_p}\left(-1 + \frac{D_p^2 \Delta\rho\, \omega^2 L\, sin^2\varphi}{18\mu_l}\right) \tag{21}$$

If at the time $t = \tau$ the droplet hits the upper disc at $y = H\, sin\varphi$ before leaving the discs' section for $x < 0$, the droplet coalesces towards the heavy phase outlet channel sliding along the upper disc. Hence, for the trajectory 2 the initial conditions are:

$$\begin{cases} x_{20} = x_{1,\tau} \\ y_{20} = y_{1,\tau} = H\, sin\varphi \\ \dot{x}_{20} = \dot{x}_{1,\tau} \\ \dot{y}_{20} = 0 \end{cases} \tag{22}$$

### A.3 Velocity profile

The fed mixture flow velocity $V_F$ is derived to determine the relative velocity subsisting between the two liquids. $V_F$ is a function of the Reynolds number and a build-up of a boundary layer at the discs' surface exists, leading to parabolic velocity profile (Plat, 1994). The expression for the velocity $V_F$ assuming a parabolic profile can be found as in (Plat, 1994). The mixture flow velocity $\tilde{V}_F$ can be expressed as function of $x$ (Di Pretoro and Manenti, 2020):

$$\tilde{V}_F = \frac{Q}{2\pi nx H\, sin\varphi} \tag{23}$$

And for a parabolic velocity profile and for $0 \le y \le H\, sin\varphi$:

$$V_F(x,y) = \tilde{V}_F(x)\frac{y}{H\, sin\varphi}\left(1 - \frac{y}{H\, sin\varphi}\right) \tag{24}$$

Integrating between 0 and $H\, sin\varphi$ and manipulating the equations it results:

$$V_F(x,y) = \frac{3QL}{\pi nx H^2 sin^2\varphi}yL\left(1 - \frac{y}{H\, sin\varphi}\right) \tag{25}$$

## Appendix B

### B.1 Mathematical model - hypotheses evaluation

The hypotheses behind the developed centrifuge mathematical model covered in section 2.2.1 are evaluated. Firstly, all the droplet sizes are collected with the developed model, verifying the hypothesis of full fuels' separation. Among the hypotheses, Coriolis and shear forces were neglected. This assumption holds for the obtained

separator design. Both forces are insignificant compared to the centrifugal force ($F_\omega$). Starting with the Coriolis force ($F_{cor}$), its ratio with the centrifugal force equals (Plat, 1994):

$$\frac{F_{cor}}{F_\omega} = \frac{\rho_l \omega D^2}{9\mu_h} \tag{26}$$

With the methanol droplet's diameter ($D_p$) ranging 5-100 $\mu m$, the above ratio equals 0.00025-0.0921.
Regarding the shear force, this is dictated by the lift forces (($F_L$)) due to droplets' rotation. The lift-centrifugal force ratio is (Plat, 1994):

$$\frac{F_L}{F_\omega} = \frac{0.172G_s^{1/2}\rho_h gD_p sin\varphi cos\vartheta}{\omega^2 \frac{D_{TOT}}{2}\mu_h^{1/2}} \tag{27}$$

Where $\vartheta$ is the angle between the lift and centrifugal forces, and unknown in this problem, while $G_S$ is the shear rate expressing the flow velocity gradient:

$$G_S = \frac{V_F(y = Hsin\varphi - D) - V_F(y = Hsin\varphi)}{D_p} \tag{28}$$

$F_L/F_\omega$ depends on the droplet's diameter and $G_S$ is implicitly a function of the flow. Hence, $F_L/F_\omega$ is calculated for the diameter at the extremes of the 5-100 $\mu m$ range and for the inlet volume flow equal to $4.076 \cdot 10^{-4}$ and $2.241 \cdot 10^{-4}$ m$^3$/s dictated by the yacht's operational modes. It results that $F_L/F_\omega$ ranges $0.00136cos\vartheta$- $0.0340cos\vartheta$. Thus, the droplet's break-up and deformation caused by shear forces can be neglected for the droplet's sizes considered and for the resulting separator design. Consequently, the assumptions employed in the model can be considered valid.